RESEARCH ARTICLE

Macromolecular Bioscience
www.mbs-journal.de

Bioink Platform Utilizing Dual-Stage Crosslinking of Hyaluronic Acid Tailored for Chondrogenic Differentiation of Mesenchymal Stromal Cells

Julia Hauptstein, Leonard Forster, Ali Nadernezhad, Hannes Horder, Philipp Stahlhut, Jürgen Groll, Torsten Blunk, and Jörg Teßmar**

3D bioprinting often involves application of highly concentrated polymeric bioinks to enable fabrication of stable cell-hydrogel constructs, although poor cell survival, compromised stem cell differentiation, and an inhomogeneous distribution of newly produced extracellular matrix (ECM) are frequently observed. Therefore, this study presents a bioink platform using a new versatile dual-stage crosslinking approach based on thiolated hyaluronic acid (HA-SH), which not only provides stand-alone 3D printability but also facilitates effective chondrogenic differentiation of mesenchymal stromal cells. A range of HA-SH with different molecular weights is synthesized and crosslinked with acrylated (PEG-diacryl) and allylated (PEG-diallyl) polyethylene glycol in a two-step reaction scheme. The initial Michael addition is used to achieve ink printability, followed by UV-mediated thiol–ene reaction to stabilize the printed bioink for long-term cell culture. Bioinks with high molecular weight HA-SH (>200 kDa) require comparably low polymer content to facilitate bioprinting. This leads to superior quality of cartilaginous constructs which possess a coherent ECM and a strongly increased stiffness of long-term cultured constructs. The dual-stage system may serve as an example to design platforms using two independent crosslinking reactions at one functional group, which allows adjusting printability as well as material and biological properties of bioinks.

1. Introduction

In recent years, biofabrication evolved as a promising and fast-growing field for applications in general life sciences as well as in regenerative medicine. Cell-compatible 3D fabrication methods such as bioprinting are used for precise patterning of bioinks consisting of living cells and bioactive hydrogel materials. Therefore, a special interest of the field focuses on hydrogels which combine cell-supportive properties with adequate 3D printability.[1–5] To facilitate the generation of 3D printed constructs with sufficient shape fidelity, frequently highly concentrated polymeric hydrogels are used as cell supportive matrices.[4,6] However, the resulting high network density and material stiffness can negatively affect cell bioactivity and the homogeneous distribution of newly produced extracellular matrix (ECM).[4,6] As an alternative approach to increased shape fidelity, thermoplastic polymers such as poly(ϵ-caprolactone) may be used as support structures for very weak hydrogels to achieve mechanically more robust composite constructs. However, the necessity of integrating these thermoplastic materials reduces the degrees of freedom in the design of an application and can distinctly impair the development of a coherent tissue within the construct.[4] Thus, a major challenge of the field is the development of hydrogels that can be applied in low polymer concentrations providing favorable conditions for the incorporated cells, but can also be adequately 3D printed into constructs without further support structures.[4,6]

For biofabrication of cartilage, hyaluronic acid (HA) represents an attractive basis for a suitable hydrogel as it is one of the major components of the extracellular matrix in human articular cartilage.[7–9] In previous non-printed approaches of HA hydrogels for cartilage engineering, ECM deposition with only limited spatial distribution depended mainly on hydrogel network density.[10–14] Reduction of the polymer concentration has led to an improved ECM distribution,[10–12] but this has yet to be transferred to printable systems. For 3D bioprinted constructs, several differently modified HA-based bioinks were used that were not stand-alone printable and needed an additional support

J. Hauptstein, H. Horder, T. Blunk
Department of Trauma, Hand, Plastic and Reconstructive Surgery
University of Würzburg
97080 Würzburg, Germany
E-mail: blunk_t@ukw.de

L. Forster, A. Nadernezhad, P. Stahlhut, J. Groll, J. Teßmar
Chair for Functional Materials in Medicine and Dentistry and Bavarian Polymer Institute
University of Würzburg
97070 Würzburg, Germany
E-mail: joerg.tessmar@fmz.uni-wuerzburg.de

The ORCID identification number(s) for the author(s) of this article can be found under https://doi.org/10.1002/mabi.202100331

DOI: 10.1002/mabi.202100331

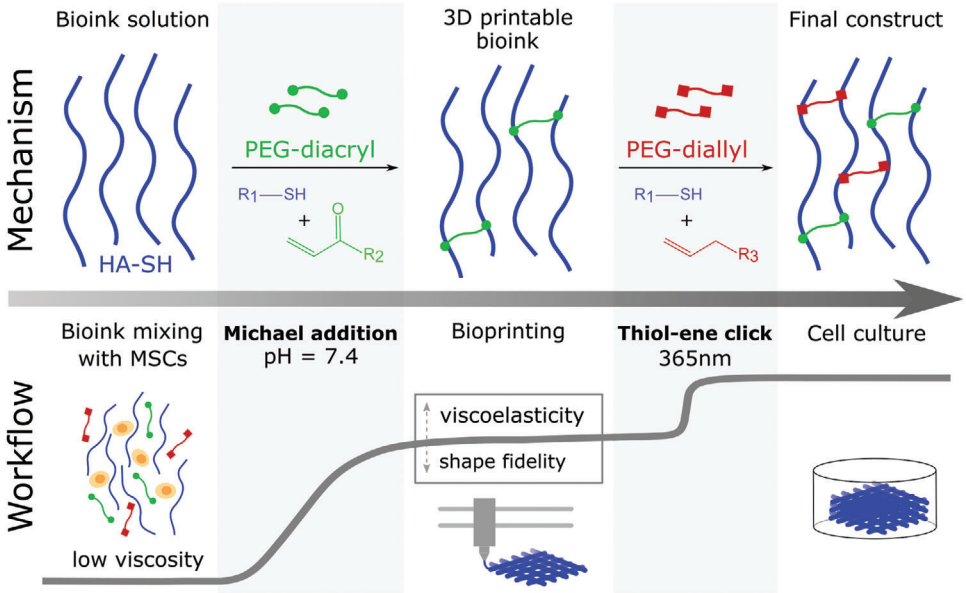

Figure 1. Dual-stage crosslinking of the hyaluronic acid-based bioinks. Mechanism: HA-SH (blue) pre-crosslinks with PEG-diacryl (green) in a spontaneous Michael addition at neutral pH to a 3D printable ink. Final crosslinking of the printed constructs is performed by UV-induced thiol–ene click chemistry between the remaining HA-SH thiol groups and PEG-diallyl (red) in the presence of the photoinitiator Irgacure (I2959). Workflow: All bioink components are mixed with MSCs in a low viscosity suspension. After appropriate pre-crosslinking, the viscoelastic bioink can be printed with improved shape fidelity. Final crosslinking is achieved via UV initiated thiol–ene click reaction leading to stable constructs, which subsequently can be subjected to cell culture.

structure for construct stabilization.[15–18] However, flexible stand-alone HA hydrogel systems which show a high initial shape stability after printing as well as favorable conditions with regard to viability of mesenchymal stromal cells (MSC) and long-term chondrogenic differentiation are still rare. Recent publications confirmed the general interest in such HA bioinks for MSC culture and demonstrated printability. However, biological characterization mostly did not exceed visual demonstration of cell viability.[7,19,20] A promising approach to enable support-free bioprinting appears to be dual-stage crosslinking of HA, as it provides an extrudable ink after a first weak or reversible crosslinking step and terminal construct stability after final crosslinking. Similar approaches have already been studied also for hydrogels used for wound closure applications.[21] In previous studies attempting dual-stage crosslinking of bioinks, printability has been achieved via thermo reversible gelation,[22] reversible guest-host assembly,[23] or weak enzymatic pre-crosslinking of attached tyrosine units,[24] each followed by a final crosslinking step via UV or visible light irradiation to guarantee the required network stability for cell culture. Again, these approaches presented printable materials, but lacked extended biological characterizations, as they analyzed only short-term viability of embedded cells.

Therefore, in this study we aimed to develop a new versatile HA bioink platform based on a dual-stage crosslinking approach, which provides not only stand-alone 3D printability after the first crosslinking step but also favorable conditions after terminal crosslinking for long-term chondrogenic differentiation of MSCs, with a focus on the distribution of newly produced ECM. A range of thiolated HA (HA-SH) with different molecular weights was synthesized and crosslinking was achieved in two stages, utilizing adjustable amounts of polyethylene glycol-diacrylate (PEG-diacryl) for pre-crosslinking and polyethylene glycol-diallyl carbamate (PEG-diallyl) for thiol–ene mediated post-crosslinking after 3D printing. In general, a distinctly lower total polymer content was needed for the more viscous high molecular weight HA-SH (>200 kDa), to achieve an optimal 3D printability of the inks, as compared to low molecular weight HA-SH (≈50 kDa). In long-term cell culture over 21 d, MSCs were demonstrated to differentiate chondrogenically in all bioprinted constructs. Bioinks with 51 kDa HA-SH required a high polymer content for good printability but resulted in only pericellular ECM distribution and overall weak mechanical properties of the final constructs after chondrogenic differentiation. In contrast, constructs made from 230 and 410 kDa HASH, needing only a low polymer content for 3D printing, exhibited higher GAG and collagen (COL) contents, a homogeneous ECM distribution throughout the constructs, and strongly improved stiffness after chondrogenic differentiation. The study contributes to effective bioink development leading to improved biological properties of bioprinted constructs.

2. Results and Discussion

This study presents a new category of hyaluronic acid-based bioinks for 3D printing using a novel dual-stage crosslinking mechanism (**Figure 1**), based on thiol-modified hyaluronic acid (HA-SH) and the cross-linkers PEG-diacryl and PEG-diallyl. The cells are suspended in the ink precursor solution containing HA-SH and both cross-linkers. The first crosslinking step (pre-crosslinking) is a spontaneous Michael addition at pH = 7.4, where HA-SH is partially crosslinked with PEG-diacryl at 37 °C to a shear thinning and 3D printable ink (Figure 1). The viscoelas-

tic properties of the ink and the shape fidelity of the printed constructs can be adjusted by altering the molecular weights of HA-SH and PEG-diacryl or by shifting the HA-SH/PEG-diacryl ratio. Depending on the ink composition, the 3D printing process can be started after 1 h of pre-crosslinking and conducted within a processing window of around 2 h. After printing, the second crosslinking step is induced in presence of the photoinitiator Irgacure I2959 by using UV light at 365 nm. This initiates the thiol–ene click reaction of remaining HA-SH thiol groups and PEG-diallyl, resulting in stably crosslinked constructs (Figure 1).

2.1. Synthesis and Characterization

2.1.1. Synthesis of 3,3′-Dithiobis(propanoic dihydrazide) (DTPH)

DTPH, required for subsequent modification of hyaluronic acid, could be synthesized in 100 g scales according to literature, with only minor changes in the purification steps as described before.[25] NMR analysis was performed in d_6-DMSO and confirmed successful synthesis and purification (Figure S1b, Supporting Information).

2.1.2. Synthesis of Thiolated Hyaluronic Acid

Educts used in the literature for HA-SH synthesis are almost exclusively of low molecular weight nature (<100 kDa), with a high solubility and low viscosity in concentrations below 1.5%, and have mostly resulted in substituted HA-SHs of <50 kDa.[16,26] To facilitate the generation of hydrogels with comparably low polymer content, HA-SH of larger molecular weights were synthesized (Figure S1a, c, Supporting Information). Therefore, transfer of the published reaction conditions[16,26] to starting materials with up to 1.4 MDa and the associated very high viscosity of 1% solutions had to be adapted to yield appropriate thiol modification and high product quality. Educts and products used in this study are listed in Table S1 (Supporting Information). Product quality was substantially improved by addition of N-hydroxy succinimide (NHS) which prevents formation of an N-acylureate. This byproduct would inhibit accurate determination of the degree of substitution (DS) via NMR (Figure S1d,e, Supporting Information) and has unknown effects on hydrogel formation and cell biology.[27] Constant reaction parameters (pH, temperature, mixing) and thus reproducibility were achieved by using a Sørensen buffer system and a thermostated incubator.

2.1.3. Synthesis of Polyethylene glycol-Diacrylate (PEG-Diacryl)

The acrylation of linear PEG and its purification was carried out as described in literature[28] (Figure S2a, Supporting Information). Complete acrylation was possible, but contrary to the described purification, precipitation in diethyl ether was ineffective. Instead, recrystallization in ethanol led to the desired pure product and was suited to remove the organic salts formed during synthesis. Successful acrylation was demonstrated by the absence of TFA ester signals in ^{1}H-NMR (Figure S2c, Supporting Information). Molecular weights of the obtained products reflected well the used educts and showed only slight polymerization during recrystallization (Figure S2b, Supporting Information).

2.1.4. Synthesis of Polyethylene glycol-Diamine (PEG-NH_2)

The conversion of PEG-OH to PEG-NH_2 was straightforward with respect to the literature (Figure S3a–c, Supporting Information).[29] Higher yields were achieved by omitting the purification of the mesylate intermediate and by processing under constant cooling.

2.1.5. Synthesis of Polyethylene glycol-Diallyl carbamate (PEG-Diallyl)

For the synthesis of PEG-diallyl derivative, the reaction conditions for the alloc protection of amino groups in peptide synthesis were applied to the previously prepared linear PEG-diamine (Figure S3a, Supporting Information).[30] The obtained products exhibited a narrow molecular weight distribution and high purity due to volatile byproducts (Figure S3b,c, Supporting Information). Quantitative conversion was demonstrated by ^{1}H-NMR using the same analysis as for PEG-diacryl (Figure S3d, Supporting Information).

2.2. Ink Development

2.2.1. Influence of HA-SH and PEG-Diacryl Properties on 3D Printability

As a first step of bioink development, the pre-crosslinking mechanism via Michael addition (Figure 1) was established for HA-SH batches of different molecular weights with 6 kDa PEG-diacryl. The aim was to get stably printable inks after a cell-compatible crosslinking time. Therefore, HA-SH and PEG-diacryl were mixed in varying concentrations, and the solutions were examined for their viscosity over time in handling experiments by pipetting or extrusion at a bioprinter, revealing an optimal printability when mixing HA-SH and PEG-diacryl in similar weight percentages. These results were further supported with extrudability experiments at the Z010 universal testing machine. Here, several hydrogel formulations were extruded after 1 h of pre-crosslinking at a constant feed rate and the required force as well as the obtained strands were recorded. In the following, all polymer concentrations are labeled as % and indicate weight percent. For extrudability experiments, the HA-SH (230 kDa) content was kept constant at 0.5% and the PEG-diacryl (6 kDa) concentration was varied between 0.1% and 2.0% (**Figure 2**). Ink formulations with 0.4% PEG-diacryl and below showed no increase in viscosity, but 0.5% or more resulted in hydrogels with increased viscosity. Thereby, the correlation between acrylate content and hydrogel viscosity was not of linear nature. Instead, the stiffness increased rapidly between 0.5% and 1.0% and then converged toward an upper limit at 2.0%, which corresponds to the quantitative saturation of the present thiols. Within the range of hydrogel forming formulations, only hydrogels with 0.5% and 0.75% PEG-diacryl were found to be proper-gelled and thus suitable for printing, whereas the hydrogel formulations with higher acrylate content were already over-gelled and resulted in strands of visibly sheared microgel particles. As a lower polymer content was expected to be more beneficial for the cell performance, the formulation with

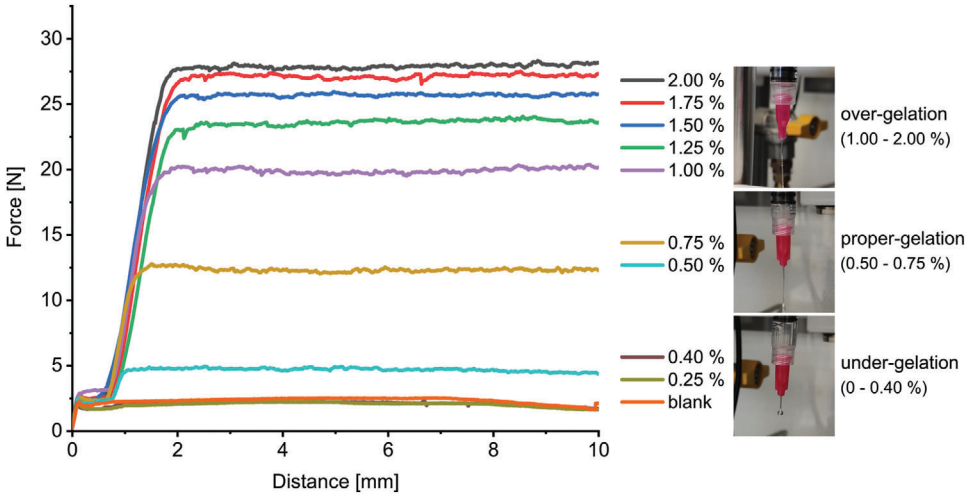

Figure 2. Force–distance diagram for an extrudability test of 230 kDa HA-SH (0.5%) hydrogels formulations with different 6 kDa PEG-diacryl contents after 1 h of incubation. Pictures indicate different strand examples for each gelation state.

a 1:1 ratio (0.5% HA-SH + 0.5% PEG-diacryl) was used in further experiments. This corresponded to a HA-SH thiol saturation of around 30%. In the following, an extended series of formulations was investigated with a constant 1:1 ratio but different polymer contents (0.1%–3.25% each), based on six differently sized HA-SH batches (M_W = 51–410 kDa) and 6 kDa PEG-diacryl, in which the components were mixed, and the viscosity was assessed over time. **Figure 3**a represents a summarized overview of the investigated formulations with different HA-SH/PEG-diacryl concentrations and the suitability for 3D printing. Each line of the graph represents 16 different pre-crosslinking approaches, which were analyzed separately over 5 h, and all formulations resulting in sufficient strand formation already after a cell-compatible pre-crosslinking time of 1 h were defined as printable. An exemplary more detailed analysis table is presented in the Supporting Information, showing the relevant HA-SH/PEG-diacryl concentrations tested with the 410 kDa HA-SH batch (Figure S4, Supporting Information). The dependence of the processing window on the polymer content was also similarly found for all other tested HA-SH batches. Summarizing Figure 3a, a clear trend was observed: With increasing molecular weight of the HA-SH component (top to bottom), a decreasing total polymer content was necessary for optimal 3D printability of the inks. HA-SH batches with the lowest molecular weight (around 50 kDa) required a total polymer content of at least 4.5% (2.25% HA-SH + 2.25% PEG-diacryl), whereas those with molecular weights over 200 kDa required a significantly lower total polymer content to be printable after 1 h of pre-crosslinking. This was in line with observations in the literature in which the effect of the M_w of unmodified hyaluronic acid on the viscosity in aqueous solutions has been investigated.[31] Interestingly, no further reduction of polymer content was possible when increasing the M_w from 230 kDa to the highest achieved M_w of 410 kDa.

As a next step, the impact of PEG-diacryl molecular weight on ink printability was assessed. Therefore, three HA-SH batches (51, 230, and 410 kDa) were selected. The HA-SH concentration was fixed while concentrations of 6, 10, and 20 kDa PEG-diacryl were varied. Figure 3b shows exemplarily the results for the 410 kDa HA-SH batch. The PEG content needed for adequate 3D printability increased with the molecular weight of PEG-diacryl. The same trend was also observed for the 51 and 230 kDa HA-SH batches (Figure S5, Supporting Information). These observations can be explained by the fact that PEG-diacryl with increased molecular weight requires a higher concentration to provide the same amount of acrylate groups. Accordingly, stoichiometric calculations revealed again around 30% HA-SH thiol saturation for all printable formulations.

2.2.2. Thiol–Ene Crosslinking of the Printed Bioink Using PEG-Diallyl

The final crosslinking of printable ink formulations (Figure 1, second viscosity increase) was conducted with 6 kDa PEG-diallyl in the presence of the photoinitiator Irgacure (I2959) at 365 nm. The concentrations of PEG-diallyl were determined by stoichiometric calculations to achieve a complete thiol saturation for the different HA-SH batches. For the following detailed physicochemical and biological characterizations, three inks with different HA-SH batches (51, 230, and 410 kDa) were produced. Each HA-SH was pre-crosslinked with 6 kDa PEG-diacryl and finally gelated with 6 kDa PEG-diallyl. The exact ink compositions were in accordance with the printability studies shown in Figure 3 and are listed in **Table 1**. In the following, these inks are termed as 51, 230, and 410 kDa HA-SH inks. To evaluate potential effects of each crosslinking process, MSC cell viability was analyzed after pre-crosslinking as well as after final UV irradiation. Quantification revealed 95%–98% cell survival for both crosslinking steps in all three bioinks without significant differences between the conditions (Figure S6, Supporting Information), demonstrating no detrimental influence of the crosslinking processes.

2.2.3. Rheological Characterization of the Dual-Stage Crosslinking

Rheological properties of the inks play a significant role in their applicability to extrusion-based bioprinting. In this context, viscoelastic features of the hydrogels are highly dependent on the

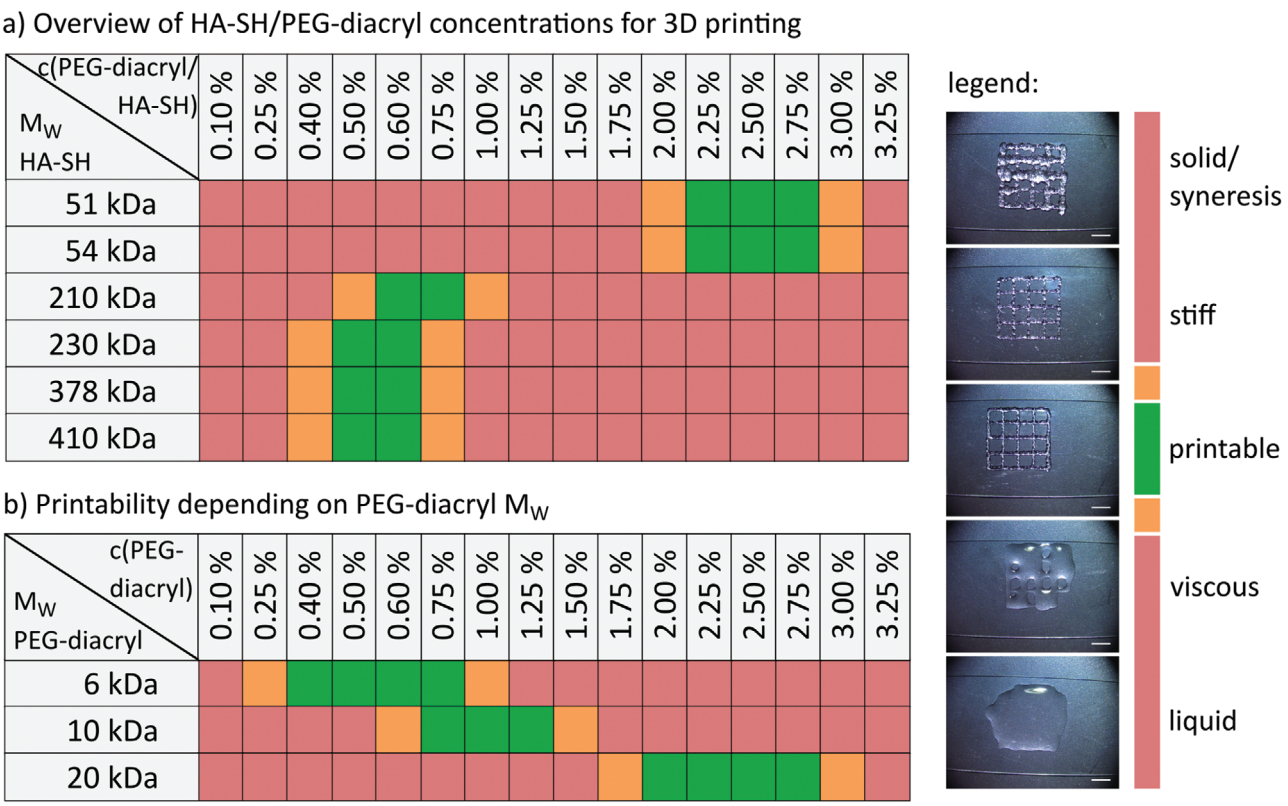

Figure 3. Processing windows of different HASH/PEG-diacryl molecular weights and concentrations. All mixtures resulting in sufficient strand formation after a cell-compatible pre-crosslinking time of 1 h are defined as printable. The general printability is visualized by a color code (green = printable, red = not printable (either too liquid, viscous, stiff, or too solid) and yellow marks the transition region). The legend depicts exemplary printed grids for each condition. Scale bars represent 5 mm. a) Six different HA-SH batches (MW = 51–410 kDa) were tested with PEG-diacryl (6 kDa) in 1:1 ratios (0.1%–3.25% each) and printability of the resulting polymer solutions was analyzed over 5 h. b) Influence of PEG-diacryl molecular weight on ink printability. 0.5% HA-SH (410 kDa) was mixed in different ratios with PEG-diacryl (6, 10, and 20 kDa) and printability of the resulting solutions was analyzed over 5 h.

Table 1. Compositions of inks used in all further experiments. All values are represented as % (wt V^{-1}).

HA-SH batch (kDa)	*c*(HA-SH) (%)	*c*(PEG-diacryl) (%)	*c*(PEG-diallyl) (%)	*c*(Irgacure) (%)
51	2.5	2.5	5.0	0.05
230	0.5	0.5	1.0	0.05
410	0.5	0.5	1.0	0.05

molecular weight as well as polymer content of the ink formulations. Moreover, progression of crosslinking reactions and kinetics of gel formation depend on chain mobility and availability of functional groups. A series of rheological experiments was performed to investigate the kinetics of the gelation in different ink formulations and to evaluate the processing window for application of such inks (**Figure 4**). Pre-crosslinking via Michael addition at 37 °C for the three different inks, 51, 230, and 410 kDa HA-SH led to increased storage and loss moduli after an initial induction period (Figure 4a). The molecular weight of HA-SH as well as the polymer content played a significant role in the reaction kinetics. Decreasing the molecular weight at the same concentration (410 kDa vs 230 kDa, Table 1) resulted in slower crosslinking kinetics. This could be explained by the availability of functional groups per polymer chain, considering that the degree of substitution in both ink formulations was nearly identical (Table S1, Supporting Information). Thus, decreasing the molecular weight of the polymer caused smaller number of available thiols per polymer chain for the Michael addition, which in turn formed less long-range entanglement of chains due to lower probability of network formation. On the other hand, increasing the concentration, and consequently the number of available functional groups, resulted in faster kinetics of network formation in 51 kDa HA-SH, despite having a significantly shorter chain length. In comparison to experimental observations that all inks were printable after only 1 h of incubation, obtained time sweeps showed slightly different gelation points and thus possible printability. This was explained by obvious differences in hydrogel formation.

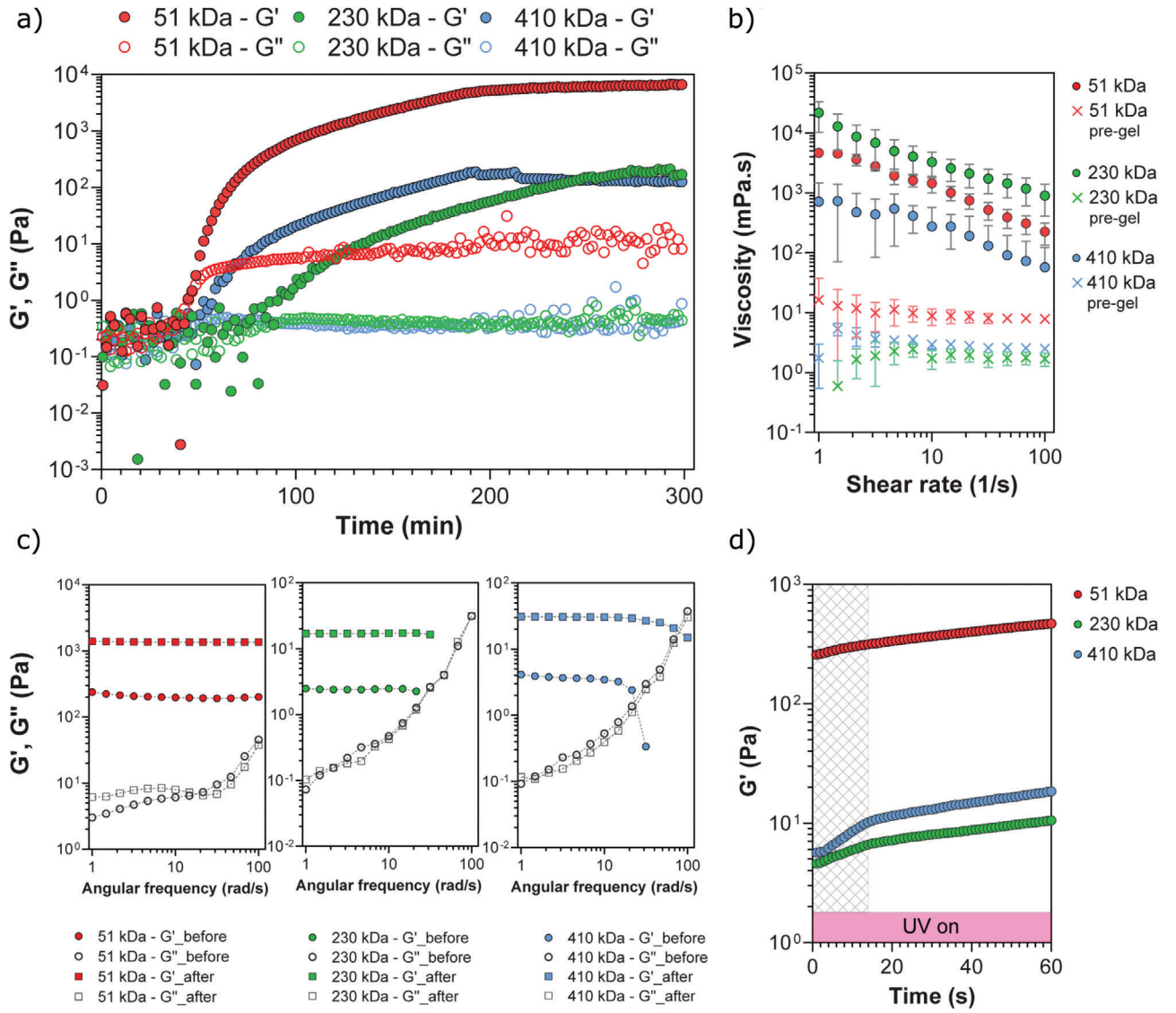

Figure 4. Rheological characterization of the different HA-SH bioinks. a) Time sweep measurements to identify the kinetics of the Michael addition and identification of the processing window of the bioinks. b) Shear rate dependence of the viscosity of HA-SH formulations before and after pre-crosslinking via Michael addition. c) Frequency sweeps of the different inks before (circle) and after (square) exposure of UV light. d) Close-up of the change in storage modulus during the 60 s UV exposure period. Dashed region indicates the initial rapid rise in elastic properties of the formed networks during photo-crosslinking.

While rheological studies were performed under almost stationary conditions, in extrudability experiments the hydrogel formulations were frequently mixed during incubation and thus, had a higher probability of network formation. For all tested bioinks, a steady slow increase in G' was observed after the initial steep rise, which was attributed to the formation of additional disulfide bonds from unsaturated thiols. Disulfide formation is a spontaneous process in systems based on thiol chemistry that is much slower than Michael addition between free thiols and acrylates of PEG-diacryl.[32] Furthermore, the growing noise in G'' after 3 h of incubation could be related to such disulfide formation resulting in hydrogel shrinkage during the measurements. Hydrogel precursor solutions showed only very weak dependency of the viscosity on applied shear, which is a characteristic of diluted polymer solutions (Figure 4b). The shear-thinning indices of pre-gel solutions were 0.88, 0.96, and 0.86 for formulations based on 51, 230, and 410 kDa HA-SH, respectively. The shear-dependent viscosity behavior of formulations after the first stage of crosslinking was more evident, as all the formulations showed strong pseudoplastic behavior with flow indices of 0.33, 0.38, and 0.58 for formulations based on 51, 230, and 410 kDa HA-SH, respectively. This behavior confirmed the shear rate dependency of the viscosity of the bioinks after the first stage of crosslinking, which would facilitate an appropriate extrusion through a fine nozzle with a sufficient shape fidelity.

For the second crosslinking stage, involving a thiol–ene click reaction, the network viscoelasticity before, after, and during the photo-crosslinking by UV light was monitored (Figure 4c,d). The

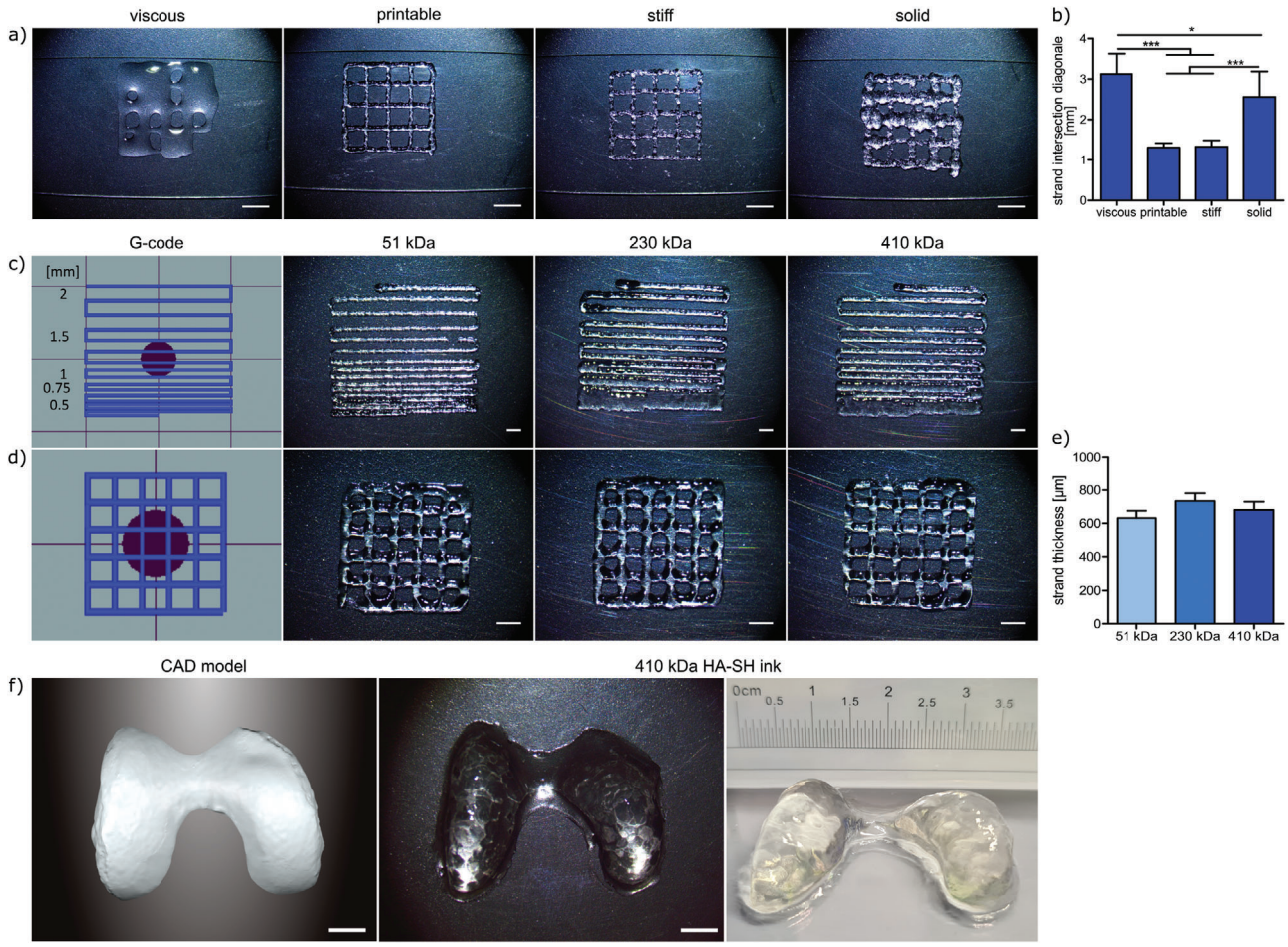

Figure 5. Shape fidelity of 3D-printed HA-SH inks. a) 3D printed grids with different HA-SH ink compositions, leading to viscous, printable, stiff, and solid inks, respectively (images were also used in the legend of Figure 3). Scale bars represent 5 mm. b) Quantification of the strand intersection diagonal of printed grids in (a). c) G-code and filament fusion tests of 51, 230, and 410 kDa HA-SH inks. Scale bars represent 2 mm. Strand distance of the printed filament is indicated next to the G-code. d) G-code and printed grids of the same inks. Scale bars represent 2 mm. e) Quantification of the strand thickness. f) CAD model of the human right femur condyles (left) and the real construct exemplarily printed with 410 kDa HA-SH in 21 layers (middle: top view, right: side view). Scale bars represent 5 mm.

frequency sweeps prior to and after the photo-crosslinking stage showed a distinct increase of the storage modulus, i.e., an enhancement in viscoelastic properties of inks, through development of longer interaction ranges, as well as shifting of the relaxation time of the network to higher frequency values (Figure 4c). Two distinguishable regions within the period of UV light exposure were identified (Figure 4d). The increase in storage modulus within the first 15 s of exposure was higher compared to the remaining exposure period, and the difference was greater for inks with longer HA-SH chains. The initially differing growth rates for the different inks converged in the second region, resulting in a steady increase of the storage modulus until the end of UV exposure. This corresponds to the quantitative thiol saturation via thiol–ene reaction and thus to the intended terminal plateau of viscoelasticity in the workflow of ink processing (Figure 1). The higher increase rate for G' of longer polymer chains in Figure 4d was attributed to a higher number of available thiol groups per polymer chain, which resulted in more efficient polymer immobilization and consequently, entanglement and formation of long-range interactions.

2.3. Printability Assessment

In the following, a detailed printability characterization of the platform bioinks was performed. At first, the strand intersection diagonal of grid constructs printed with a viscous, printable, stiff, and solid ink composition—corresponding to the color code in Figure 3—was analyzed and quantified (**Figure 5**a,b). 3D printing of viscous and solid inks was characterized by a large and inconsistent intersection diagonal, while printable and stiff inks yielded uniform constructs with an intersection diagonal of around 1.3 mm. The printable compositions of 51, 230, and 410 kDa HA-SH inks (Table 1) were furthermore printed in a filament fusion test, with narrowing strand distances of 2, 1.5, 1, 0.75, and 0.5 mm (Figure 5c). Only the smallest distance of

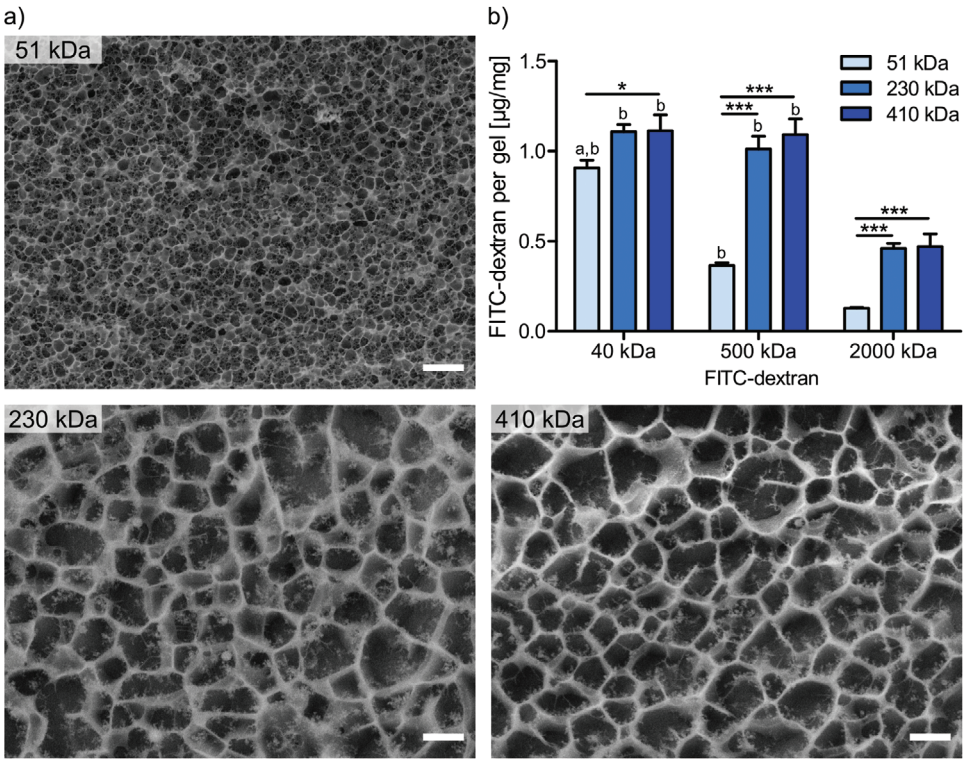

Figure 6. a) Pore structure visualization selected inks by cryo-SEM imaging. Scale bars represent 2 µm. b) Analysis of diffusion of FITC-labeled dextrans (40, 500, and 2000 kDa) into the HA-SH constructs. Data are represented as mean ± standard deviation ($n = 3$). Significant differences are marked as follows: $^{*}p < 0.05$, $^{**}p < 0.01$, and $^{***}p < 0.001$. a) Significantly different to the corresponding group incubated in 500 kDa FITC-dextran solution, b) significantly different to the corresponding group incubated in 2000 kDa FITC-dextran solution (at least $p < 0.05$).

0.5 mm led to strand fusion. All other distances were well printable using a 330 µm nozzle. The same inks were also printed in grid structures (Figure 5d) and the resulting strand thickness was quantified (Figure 5e). No significant differences between the different inks were detected. All printed strands yielded an average thickness between 630 and 730 µm. Finally, a large construct with 21 layers was printed with the 410 kDa HA-SH ink as a proof-of-principle experiment resembling human femoral condyles (Figure 5f).

2.4. Impact of Ink Formulation on Construct Stability, Pore Structure, and Diffusion

Construct stability of 51, 230, and 410 kDa HA-SH inks was determined in a swelling study. Therefore, constructs were prepared as described above and incubated for 21 d in phosphate-buffered saline (PBS). Weight measurements were performed, and the wet weight deviation at a specific time point compared to the weight directly after preparation was calculated (Figure S7, Supporting Information). After an initial swelling due to PBS inflow, all constructs decreased in wet weight again and reached an equilibrium weight at day 3 (≈145% for 51 kDa and ≈100% for 230 and 410 kDa). In general, all constructs maintained a constant wet weight between 3 and 21 d, indicating a stable network without degradation. The polymer content and network density can distinctly impact macromolecular diffusion within hydrogels, which in turn may modulate nutrient supply and decisively influence the ECM distribution, newly produced by incorporated cells.[10,11,15] To assess the pore structure of 51, 230, and 410 kDa HA-SH inks, cryo-scanning electron microscopy (cryo-SEM) images were taken directly after gel preparation (**Figure 6**a). The high concentrated 51 kDa ink has distinctly smaller pores than the low concentrated 230 and 410 kDa HA-SH inks. Furthermore, the impact of polymer content on diffusivity in these inks was analyzed with fluorescein isothiocyanate (FITC)-labeled dextrans of different sizes (Figure 6b). Hydrogel cylinders were incubated in three different FITC-labeled dextran solutions (40 kDa, on the order of growth factors; 500 and 2000 kDa, on the order of ECM molecules and aggregates), and diffusion into the constructs was analyzed after 24 h. Quantification in the constructs revealed unimpaired diffusion of 40 and 500 kDa FITC-labeled dextrans into the constructs with low polymer content (230 and 410 kDa HA-SH), while diffusion into the constructs with high polymer content (51 kDa HA-SH) was slightly reduced for the 40 kDa and strongly impaired for the 500 kDa FITC-labeled dextrans. The 2000 kDa dextran diffusion was reduced in all ink compositions, but again a significantly higher diffusion into the 230 and 410 kDa HA-SH constructs was detected. These results were well in agreement with the cryo-SEM images indicating a looser network with increased diffusivity in constructs with low polymer content (230 and 410 kDa).

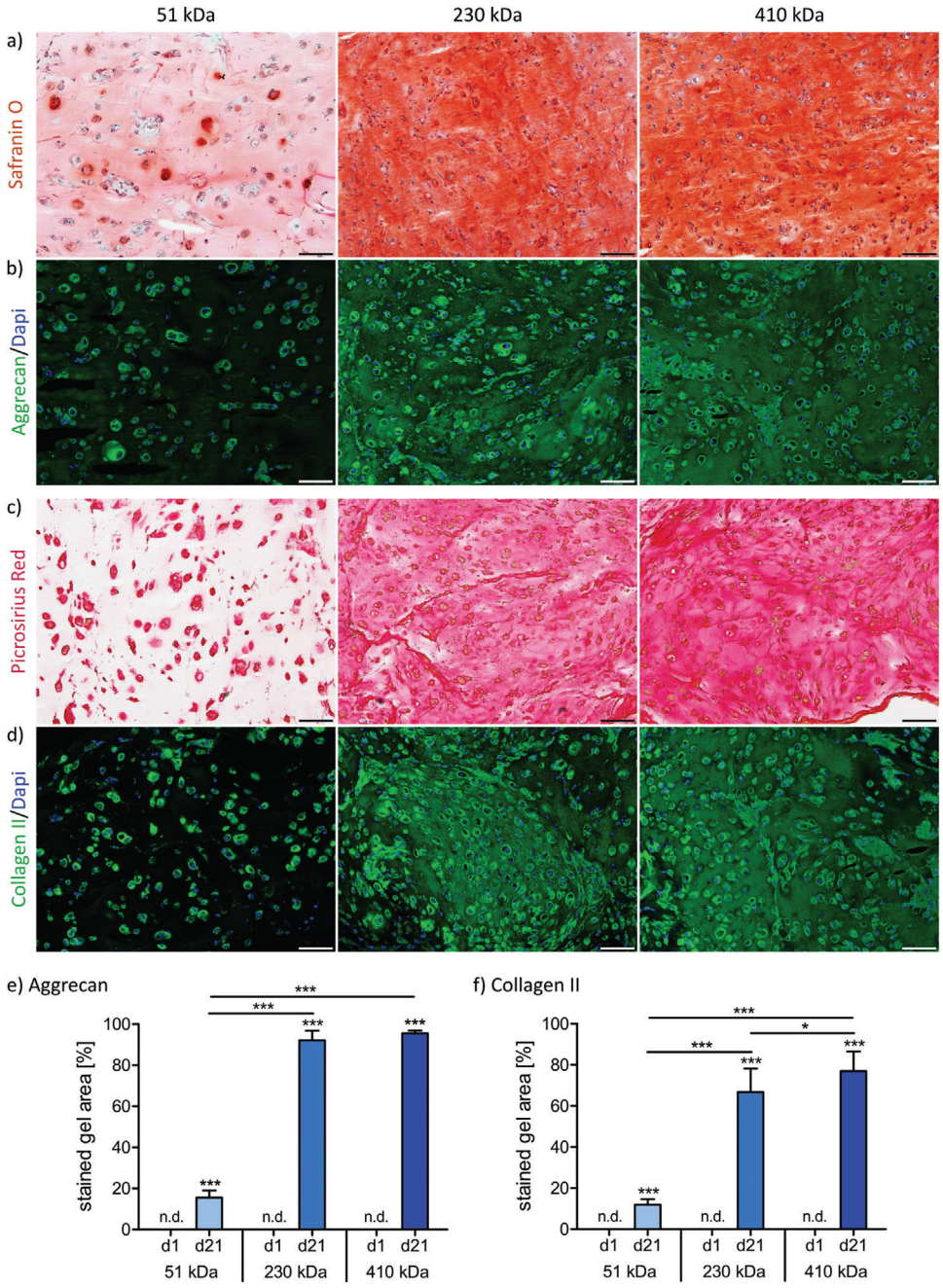

Figure 7. Histological and immunohistochemical (IHC) staining of ECM components produced by MSCs during 21 d of chondrogenic culture in 3D printed 51, 230, and 410 kDa HA-SH constructs. a) Safranin O staining of total glycosaminoglycans and b) IHC staining of aggrecan. c) Picrosirius red staining of total collagens and IHC staining of d) collagen type II. Nuclei were counterstained with DAPI (blue). Scale bars represent 100 µm. Histomorphometric analysis of e) aggrecan and f) collagen type II distribution at day 1 and 21. Data are represented as mean ± standard deviation ($n = 10$). Significant differences are marked as follows: $*p < 0.05$, $**p < 0.01$, and $***p < 0.001$).

2.5. Differential Chondrogenic Differentiation of MSCs in Platform Bioinks

2.5.1. Histological and Immunohistochemical Analysis

The three selected ink compositions were examined regarding chondrogenic differentiation of MSC. Constructs made from 51, 230, or 410 kDa HA-SH bioinks showed good cell survival on day 1 as well as after 21 d of chondrogenic differentiation, with no distinct differences between the conditions (Figure S8, Supporting Information). The production of cartilaginous ECM was supported by all constructs, which was visualized by histology and immunohistochemistry after 21 d (**Figure 7a**–d; compare Figure S9, Supporting Information, images at day 1). Safranin O

staining of glycosaminoglycans (GAG) and picrosirius red staining of collagens revealed mainly intra- and pericellular ECM deposition in the 51 kDa HA-SH gels, while the 230 and 410 kDa HA-SH constructs presented a homogeneous matrix distribution. Immunohistochemistry of the specific ECM components aggrecan and collagen type II showed similar results, and immunohistomorphometric quantification of aggrecan and collagen type II staining verified the visual observations (Figure 7e,f). Only 15% of the total area was stained for aggrecan in 51 kDa HA-SH constructs, but homogeneous distribution was observed in 230 and 410 kDa HA-SH gels (92% and 95%). A similar trend was detected for collagen type II, with 12% distribution in 51 kDa, 67% in 230 kDa, and 77% in 410 kDa HA-SH gels. The fibrocartilage marker collagen type I was also produced, albeit to a low extent (Figure S10, Supporting Information). In general, the strongly improved distribution of large ECM components in bioinks with low polymer content (230 and 410 kDa HA-SH) was well in accordance with the increased diffusion and the analyzed pore structure of these gels (Figure 6), as compared to constructs with high polymer content (51 kDa HA-SH). The small differences between aggrecan and collagen type II distribution can be explained by different sizes of the ECM components (length of collagen: 4–12 µm vs aggrecan: 0.5–4 µm) and the positive charge of collagens,[33] which might impact the free diffusion in the negatively charged HA-SH gels.

2.5.2. Biochemical Quantification and Gene Expression Analysis of ECM Components

The main cartilage ECM components were quantified in printed hydrogels in biochemical assays. Substantial amounts of GAG and COL were detected in all constructs after 21 d of chondrogenic culture, but significantly more in the 230 and 410 kDa gels, as compared with the 51 kDa HA-SH gels (**Figure 8**a,c). When normalized to DNA content, also distinctly higher GAG and COL amounts were detected for the 230 and 410 kDa bioinks (Figure 8b,d). Thus, quantification of ECM components well reflected the histological observations.

Furthermore, gene expression analysis of MSCs in 3D printed 51, 230, and 410 kDa HA-SH gels was performed on days 1, 7, and 21 of chondrogenic culture. The expression of the transcription factor SOX9, the genes of the main ECM components aggrecan (ACAN) and collagen type II (COL2A1) as well as the fibrocartilage marker collagen type I (COL1A1) were assessed by quantitative real-time PCR (qRT-PCR) and confirmed chondrogenic differentiation under all conditions (Figure 8e–h). In general, increased expression over culture time was detected for all genes and in all constructs, showing the proceeding MSC differentiation. Comparison of the constructs with low polymer content (230 kDa vs 410 kDa HA-SH gels) revealed no significant differences for all analyzed genes. SOX9 and ACAN expression on day 7 and 21, as well as COL1A1 expression on day 7, was higher in the 51 kDa HA-SH gels compared to the 230 and 410 kDa constructs. This may be attributed to the HA content in the gels, as 51 kDa HA-SH constructs contained 2.5% hyaluronic acid, while 230 and 410 kDa gels only contained 0.5%. MSC can bind to HA, e.g. via CD44 and CD168 receptors, and a higher HA concentration may increase the probability of receptor binding and thereby may promote chondrogenic gene expression.[11,34–36] Initially, the gels with high polymer content (51 kDa HA-SH) were significantly stiffer than the low concentrated ones (**Figure 9**), which also may have an impact on MSC differentiation.[10,37] Nevertheless, increased gene expression in constructs with higher polymer content did not result in increased GAG and collagen production (Figure 8a–d), which has also been reported previously in other studies for non-printed hydrogels[11] and printed constructs with thermoplastic support structure.[15]

2.6. Construct Stiffness in the Context of ECM Distribution

Another important feature of engineered cartilage is the construct stiffness of this load-bearing tissue. For this reason, the Young's moduli of printed 51, 230, and 410 kDa HA-SH constructs with embedded MSCs were analyzed on day 1 and 21 of chondrogenic differentiation. Exemplary stress–strain curves of constructs on day 21 are shown in Figure 9a and the calculated average Young's moduli on day 1 and 21 in Figure 9b. The initial Young's modulus of the gels with high polymer content (51 kDa HA-SH) was 5.1 kPa and significantly higher than that of both gels with low polymer content (0.7 kPa for 230 and 410 kDa HA-SH). However, after 21 d of chondrogenic culture, the 230 and 410 kDa HA-SH gels exhibited a strong increase of the Young's modulus to 52.6 and 54.6 kPa, respectively, while the 51 kDa HA-SH gels were markedly weaker (4.2 kPa). This corresponded to a 0.8-fold decreased 51 kDa HA-SH construct stiffness, but a significantly increased constructs stiffness of around 73- and 74-fold over 21 d of culture time for the 230 and 410 kDa HA-SH gels (Figure 9c). The initially higher stiffness of the 51 kDa HA-SH gels was attributed to the higher polymer content (10%) (Table 1) and the resulting high crosslink density, whereas the gels with low polymer content (2%) with their loosely crosslinked networks appeared softer. Within 21 d of chondrogenic differentiation, MSCs produced considerable amounts of cartilaginous ECM under all conditions, but significantly more in 230 and 410 kDa HA-SH gels (Figures 7 and 8a–d). Even more importantly, a homogeneous ECM distribution was observed in 230 and 410 kDa HASH gels (Figure 7), facilitated by a looser hydrogel network and an enhanced diffusivity (Figure 6). This allowed for increased interaction of the produced macromolecules which is considered a likely explanation for the strong increase in construct stiffness, as shown previously.[11,15] In contrast, ECM deposition in 51 kDa HA-SH gels appeared only pericellularly (Figure 7) due to the high polymer content, which resulted in a tight network and low diffusivity (Figure 6). This prevented the distribution of ECM molecules and an increase of the Young's modulus over time. The results underscored the correlation between diffusivity, distribution of cartilaginous ECM, and construct stiffness, which has also been demonstrated in a recent study that indicated a homogeneous distribution to be even more important for construct stiffness than the bare amounts of produced ECM components.[15]

3. Conclusion

In this study, we established a flexible platform of hyaluronic acid-based bioinks for 3D printing of hMSCs which facilitated

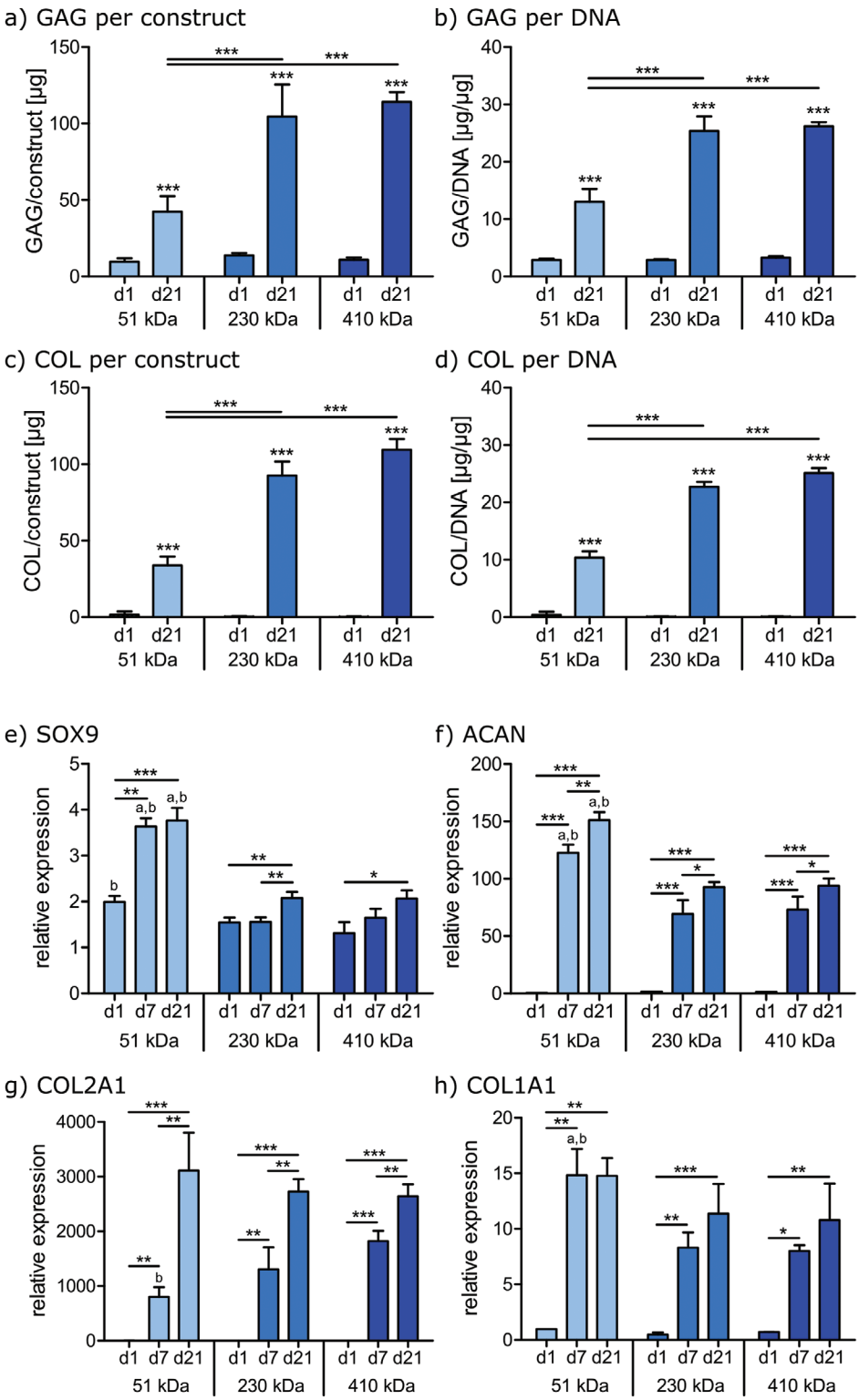

Figure 8. Quantification of glycosaminoglycan (GAG) and collagen (COL) production of MSCs cultured in 3D printed 51, 230, and 410 kDa HA-SH constructs at day 1 and after 21 d. GAG content was quantified a) in the constructs and b) per DNA. Likewise, COL production was quantified c) in the constructs and d) per DNA. Chondrogenic gene expression of MSCs in the same constructs determined by qRT-PCR. Samples at day 1, 7, and 21 were analyzed for e) SOX9, f) ACAN, g) COL2A1, and h) COL1A1 gene expression and normalized to the housekeeping gene GAPDH and to gene expression of 2D MSCs at day 0. a) Significant differences to 230 kDa HA-SH gels at the same day, and b) significant differences to 410 kDa HA-SH gels at the same day (at least $p < 0.05$). Data for both studies are represented as mean ± standard deviation ($n = 3$). Significant differences are marked as follows: *$p < 0.05$, **$p < 0.01$, and ***$p < 0.001$.

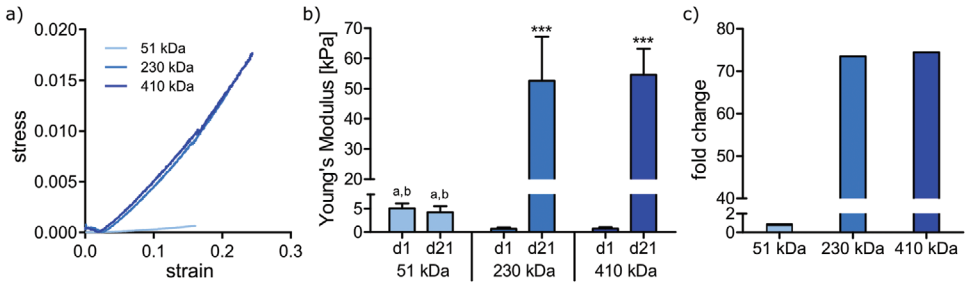

Figure 9. a) Representative stress–strain curves at day 21 and b) Young's modulus of 3D printed 51, 230, and 410 kDa HA-SH constructs with embedded MSCs on day 1 and after 21 d of chondrogenic culture. Data are represented as mean ± standard deviation ($n = 7$). Significant differences are marked as follows: Stars (***) above bars of groups at day 21 indicate significant differences to the corresponding values of the same group at day 1, $p < 0.001$. a) Significant differences to 230 kDa HA-SH gels at the same day, and b) significant differences to 410 kDa HA-SH gels at the same day (at least $p < 0.05$). c) Fold-change in Young's modulus during 21 d of chondrogenic differentiation.

a distinct modulation of the quality of cartilaginous constructs. The bioink platform uses a novel dual-stage crosslinking mechanism based on a single type of modified hyaluronic acid (HA-SH) with two independent polymeric PEG cross-linkers for Michael addition (pre-crosslinking) and thiol–ene click chemistry (final crosslinking). In contrast to formulations with low molecular weight HA-SH, bioinks prepared with high molecular weight HA-SH yielded low concentrated hydrogels with a loose porous network and allowed for enhanced macromolecular diffusion. This led to a homogeneous distribution of key ECM components aggrecan and collagen type II throughout the constructs and, thereby, resulted in a marked increase of Young's modulus over time. The principle that HA hydrogels with low polymer content allow for an improved ECM distribution compared to gels with high polymer content has been previously shown for non-printed hydrogels[10,11] and for constructs printed with an additional PCL support structure.[15] The current study transferred this to 3D constructs that are printable without the requirement of an additional thermoplastic support, which is regarded as a distinct extension of the biofabrication window.[4,6]

Taken together, these platform bioinks combine 3D printability with chondrogenic differentiation of MSC, characterized by homogeneous ECM distribution and distinctly increased construct stiffness, and therefore represent a promising perspective for cartilage regeneration. Based on the established bioink platform, future studies may include investigation of the effects of different PEG-acryl geometries or other acrylated polymers on 3D printability, and different molecular weights or geometries (e.g., four-arm or eight-arm PEG-allyl) or other allylated polymers to fine-tune the resulting hydrogel stiffness after irradiation. Overall, the developed dual-stage system may serve as an example to design bioink platforms using two independent crosslinking reactions at one functional group, which allows adjusting 3D printability as well as material and biological properties of the printed bioinks in a wide range. Here, the presented platform based on thiolated HA was tailored for cartilage engineering but may provide a high flexibility also for other applications in biofabrication.

4. Experimental Section

Materials: All chemicals were purchased from Sigma Aldrich (St. Louis, MO) if not stated differently. Acryloyl chloride stabilized with phenothiazine (abcr GmbH, Karlsruhe, Germany), 1-(3-dimethylaminopropyl)-3-ethylcarbodiimide HCl (EDC, Biosynth CarboSynth, Compton, UK), 1,4-dithiothreitol (DTT, Biosynth CarboSynth, Compton, UK), 2-hydroxy-1-[4-(hydroxyethoxy)-phenyl]-2-methyl-1-propanone (I2959; BASF, Ludwigshafen, Germany), 4-(dimethylamino)benzaldehyde (DAB; Carl Roth, Karlsruhe, Germany), basic fibroblast growth factor (bFGF; BioLegend, London, UK), chloroform-d^1 (Eurisotope, St-Aubin Cedex, France), DAPI mounting medium ImmunoSelect (Dako, Hamburg, Germany), deuterium oxide (Deutero GmbH, Kastellaun, Germany), regenerated cellulose dialysis tubes MWCO 3500 Da (Carl Roth, Karlsruhe, Germany), diethylether (Chemobar University of Würzburg, Würzburg, Germany), dimethyl-3,3′-dithiodipropionate (TCI Chemical Industry Co. Ltd., Tokyo, Japan), di-potassium hydrogen phosphate (Merck KGaA, Darmstadt, Germany), di-sodium hydrogen phosphate (Merck KGaA, Darmstadt, Germany), Dulbecco's modified Eagle's medium high glucose 4.5 g L^{-1} (DMEM; Thermo Scientific, Waltham, MA), DMEM/F12 (Thermo Scientific, Waltham, MA), ethanol (99%, TH Geyer, Renningen, Germany), fetal calf serum (FCS; Thermo Scientific, Waltham, MA), formaldehyde (37%, Carl Roth, Karlsruhe, Germany), hyaluronic acid sodium salt (M_w 1–2 MDa; 0.2–0.5 MDa; 0.08–0.1 MDa; Biosynth CarboSynth, Compton, UK), hydrochloric acid (HCl; 32%, 37%, Merck KGaA, Darmstadt, Germany), isopropanol (VWR, Radnor, PA), ITS+ premix (Corning, New York, NY), L-hydroxyprolin (Merck KGaA, Darmstadt, Germany), live/dead cell staining kit (PromoKine, Heidelberg, Germany), methanol (Fisher Scientific, Schwerte, Germany), N-hydroxysuccinimide (NHS, Biosynth CarboSynth, Compton, UK), papain (Worthington, Lakewood, CA), penicillin-streptomycin (PS; 100 U mL^{-1} penicillin, 0.1 mg mL^{-1} streptomycin; Thermo Scientific, Waltham, MA), perchloric acid (60%, Merck KGaA, Darmstadt, Germany), PBS (Life Technologies, Carlsbad, CA), potassium dihydrogen phosphate (Merck KGaA, Darmstadt, Germany), Proteinase K (Digest-All 4, Life Technologies, Carlsbad, CA), sodium hydrogen carbonate (Merck KGaA, Darmstadt, Germany), sodium hydroxide (Merck KGaA, Darmstadt, Germany), Tissue Tek O.C.T. (Sakura Finetek, Tokyo, Japan), toluene (Fisher Scientific, Schwerte, Germany), transforming growth factor $\beta 1$ (TGF-$\beta 1$; BioLegend, London, UK), tris(carboxyethyl)phosphine HCl (TCEP, Biosynth CarboSynth, Compton, UK), and trypsin-EDTA (0.25%, Life Technologies, Carlsbad, CA).

Methods: Synthesis of DTPH: The synthesis was performed according to Vercruysse et al.[25] with slight modifications. Dimethyl-3,3′-dithiodipropionate (82 mL, 1 eq.) was dissolved in 1 L methanol at rt. The clear solution was cooled to 0 °C by an ice bath and an excess of hydrazine monohydrate (8.0 eq.) was added. The clear, yellowish reaction solution was stirred at 0 °C for 4 h and then stirred overnight at rt to form a shiny, yellowish suspension. Afterward, the clear, yellow supernatant was discarded, and the precipitate was washed with methanol. Remaining methanol was removed by washing the precipitate with an excess of diethyl ether. The final product was dried in vacuo at rt to give a shiny, white solid.

Synthesis of Thiolated Hyaluronic Acid: The synthesis was performed according to Stichler et al.[16] with several modifications. HA of different molecular weights (3 g, 1.0 eq.) (Table S1, Supporting Information) was dissolved in 300 mL deionized water overnight at 37 °C to give a viscous, clear solution. NHS (4.0 eq.) and DTPH (4.0 eq.) were dissolved in 300 mL Sørensen buffer (0.2 M, pH 5.5) at rt and mixed with the HA solution. After the addition of EDC (7.5 eq.) the pH was adjusted to 4.0 with 10% HCl and the mixture was incubated for 4 h at 37 °C. The pH of the resulting clear gel was raised to over 8.5 with 2 N NaOH and DTT (5.0 eq.) was added. The mixture was incubated overnight at 37 °C to form a clear, brownish solution. Afterward, the pH was adjusted to 3.0 with 10% HCl, and the mixture was dialyzed (MWCO 1 kDa) against K_2HPO_4/HCl buffer (0.3×10^{-3} M, pH 5.0) with the addition of ascorbic acid/TCEP (each 1 g/15 L) for 3 d, then against K_2HPO_4/HCl buffer (0.3×10^{-3} M, pH 5.0) 2 d without TCEP. The obtained clear solution was freeze-dried to give a white foamy solid.

Synthesis of Polyethylene glycol-Diacrylate: The acrylation of PEG was identically performed for all three linear PEGs (6, 10, 20 kDa) according to Cruise et al.[28] First, PEG (100 g, 1.0 eq.) was molten at 110 °C and high vacuum was applied for 2 h to remove residual water. The clear melt was dissolved in 1 L of dry toluene under argon atmosphere. Dry triethylamine (3.0 eq.) was added, followed by a stepwise addition of freshly distilled acryloyl chloride (3.0 eq.). The turbid, yellow reaction solution was stirred overnight at rt to form an orange suspension. After centrifugation, the sediment was discarded and the clear, orange supernatant was cooled to 0 °C. The resulting precipitate was obtained by centrifugation and recrystallized in ethanol until discoloration of the solid phase. The purified product was dried in vacuo at rt and a white solid was obtained.

Synthesis of Polyethylene glycol-Diamine: The amination of PEG was carried out according to Iijima et al.[29] with slight modifications. Linear PEG (100 g, 1.0 eq.) was dried under high vacuum at 110 °C for 2 h, cooled to rt under argon atmosphere, and dissolved in 900 mL dry dichloromethane. Triethylamine (3.0 eq.) was added, and the clear solution was cooled to 0 °C in an ice bath. After the stepwise addition of methanesulfonyl chloride (3.0 eq.), the clear, yellow reaction solution was stirred for 1 h at 0 °C and then 4 h at rt. The solvents were removed with a rotary evaporator at 50 °C and the orange solid dissolved in 100 mL deionized water. 500 mL of a 30% ammonium hydroxide solution were added, and the clear, yellow reaction solution was stirred 3 d at 0 °C followed by 1 d at rt. Remaining ammonia was evaporated overnight in the fume hood and the clear solution was alkalified to pH 9–10 with 2 N NaOH. The aqueous layer was washed with diethyl ether (3 × 150 mL) and then extracted with dichloromethane (6 × 150 mL). The combined organic layer was dried over $MgSO_4$, concentrated in vacuo, and precipitated in cold diethyl ether. The sediment was dried in high vacuum to give a yellowish solid.

Synthesis of Polyethylene glycol-Diallyl carbamate: Linear PEG-diamine (10 g, 1.0 eq.) was dissolved in 100 mL deionized water and 8.67 mL 2 N NaOH (5.0 eq.) were added. Allyl chloroformate (1.6 eq.) was added, and the resulting two-phase system was stirred intensively for 4 h at 0 °C. After washing with diethyl ether (2 × 100 mL), the aqueous layer was extracted with dichloromethane (5 × 75 mL), the organic layers were combined, dried over $MgSO_4$, and filtered. The yellowish product solution was concentrated, precipitated in cold diethyl ether, and the sediment dried under high vacuum at rt. The purified product appeared as white solid.

NMR Analysis: ^{1}H-NMR measurements of DTPH were performed at a 400 MHz Bruker Avance III HD using d_6-DMSO and ^{1}H-NMR measurements of all polymers were performed at a 300 MHz Bruker Biospin spectrometer (Bruker, Billerica, MA) using $CDCl_3$ (PEG), and D_2O (HA-SH) as solvents. The solvent peak was set to the chemical shift $\delta = 2.50$ ppm for DMSO, 7.26 ppm for $CDCl_3$, and 4.79 ppm for D_2O to which all chemical shifts refer. The percentage of thiol groups per repetition unit of HA-SH was determined by the ratio of the integrals of the thiol-carrying modification and an internal reference, the acetyl signal together with the anomeric protons of the saccharide backbone. The quantitative PEG-modification was verified by the absence of a change in the spectra after the addition of trifluoroacetic anhydride to the NMR sample solution.

GPC Analysis: A GPC System (Gel Permeation Chromatography) entirely made from Malvern (Herrenberg, Germany) with a triple detection containing a refractive index detector (VE 3580), a viscometer (270 dual detector), and a multi-angle light scattering detector (SEC-MALS 20) was used for the GPC analysis. Depending on the molecular weight of the sample, different column sets (Malvern, Herrenberg, Germany) were used. For HA-SH samples, two A6000M mixed-bed columns and for PEG samples, a set of A2000/A3000 columns were chosen. The eluent was made from deionized water containing 8.5 g L^{-1} $NaNO_3$ and 0.2 g L^{-1} NaN_3 and the columns were calibrated with PEG standards (Malvern, Herrenberg, Germany) with a range of 150 Da to 660 kDa using a MALS calibration. All HA-SH samples were dissolved in deionized water with 0.5 g L^{-1} TCEP over 6 h at rt and PEG samples were dissolved in deionized water over 6 h at rt.

Extrudability Test: For the extrudability experiments, HA-SH/PEG-diacryl solutions were prepared in syringes with a 1:1 ratio of the functional groups in different concentrations in the range of 0.1%–2.0%. After 1 h incubation at 37 °C, the syringes were placed in a custom-made setup inside a Z010 universal testing machine from Zwick Roell (Ulm, Germany) with a 2.5 kN load cell. By applying a constant crosshead displacement rate of 10 mm min^{-1}, the solutions/hydrogels were extruded through a 250 µm steel needle and the required force and the obtained hydrogel strands were monitored.

Rheological Analysis: Rheological properties of different hydrogel formulations were characterized using an Anton Paar MCR 702 rheometer (Anton Paar, Austria) with a 25 mm parallel plate geometry at a 0.5 mm gap. A solvent trap was used to minimize evaporation throughout the experiments. All experiments were performed by loading the freshly prepared hydrogel precursors on the measurement plate pre-heated at 37 °C. Four categories of experiments were performed to characterize different aspects of the hydrogels: Time sweep measurements with 0.5% strain at 10 rad s^{-1} angular frequency were conducted to identify the processing window of the inks. Shear rate sweeps from 1.0 to 100 s^{-1} were performed to evaluate the shear thinning properties. Frequency sweeps from 100 to 1.0 rad s^{-1} were performed before and after exposure to UV light. Photo-crosslinking measurements were performed by exposure to UV light (bluepoint 4, Dr. Höhnle AG, Gräfelfing, Germany) for 60 s after slightly different incubation times at 37 °C, depending on the rate of Michael reaction progression in different inks (Table S2, Supporting Information).

MSC Isolation and Expansion: For isolation of MSCs, bone marrows were recovered from the explanted femoral heads of patients undergoing elective hip arthroplasty as previously described.[16] The procedure was performed after informed consent of all patients and with the approval of the local ethics committee of the University of Würzburg (186/18). Cells were expanded at 37 °C and 5% CO_2 in DMEM/F12 supplemented with 10% FCS, 1% PS, and 3 ng mL^{-1} bFGF.

Hydrogel Preparation, 3D Printing, and MSC Culture: HA-SH was dissolved in HEPES buffer (154×10^{-3} M, pH = 7.6) to sustain a suitable pH of 7.4 for Michael addition. All other hydrogel components (PEG-diacryl, PEG-diallyl, Irgacure I2959) were dissolved in PBS and mixed in a range of different concentrations for the establishment of the necessary ratio of thiol to acryl/allyl groups for pre-/final crosslinking. Printability was assessed by manual extrusion using a displacement pipette (Gilson, Middleton, WI) or a Cellink+ 3D bioprinter (Cellink, Boston, MA). For 3D printing, G-codes for grids and filament fusion tests were generated with the HeartWare software of the same manufacturer. Strand thickness measurements were performed with the NIH ImageJ Fiji software (version 1.52a). The CAD file of the femoral condyles of a human right leg was obtained from MakerBot Thingiverse (object 5820, created by BME_Sundevil) and sliced with the HeartWare software. Hydrogel solutions were mixed with or without MSCs (passage 3–4, 20×10^6 cells mL^{-1}) and transferred to 3 cc printing cartridges (Nordson EFD, Westlake, OH), pre-crosslinked for 1 h at 37 °C, and extruded through a 330 µm steel nozzle at a printing pressure of 40–200 kPa, depending on the ink formulation. Constructs were finally crosslinked for 10 min at 365 nm (1 mW cm^{-1}, UV hand lamp with filter, A. Hartenstein, Würzburg, Germany). MSC-laden constructs prepared with 51, 230, and 410 kDa HA-SH bioinks were incubated for 21 d at 37 °C and 5% CO_2 in differentiation medium (DMEM high glucose medium supplemented with 1% ITS+ premix, 1% PS, 0.1×10^{-6} M dexamethasone,

50 μg mL^{-1} L-ascorbic acid 2-phosphate sesquimagnesium salt hydrate, 40 μg mL^{-1} L-proline and 10 ng mL^{-1} TGF-β1).

Swelling Analysis: 51, 230, and 410 kDa HA-SH gels were prepared in a defined cylindrical geometry (diameter: 5 mm, volume: 40 μL) and weighed directly after preparation (d0). Samples were transferred to PBS and incubated for 21 d at 37 °C. Weight measurements were performed after excessive PBS was removed carefully from the hydrogel surface using a filter paper. At each time point (1, 3, 5, 7, 9, 12, 14, and 21 d), wet weight deviation compared to the weight directly after preparation was calculated.

Analysis of FITC-Labeled Dextran Diffusion: 51, 230, and 410 kDa HA-SH gels were prepared in a defined cylindrical geometry (diameter: 5 mm, volume: 40 μL) to ensure comparable diffusion parameters. All constructs were equilibrated in PBS overnight before replacing the buffer with FITC-dextran solutions (40, 500, or 2000 kDa at 1 mg mL^{-1}). Diffusion was performed for 24 h at 37 °C in the dark. Afterward, constructs were briefly washed in PBS and homogenized with a TissueLyser (Quiagen, Hilden, Germany) for 5 min at 25 Hz. Fluorescence intensity was measured with a spectrofluorometer (Infinite M200 Pro, Tecan, Crailsheim, Germany; Ex/Em 495 nm/535 nm). Quantification was performed using a 40, 500, or 2000 kDa FITC-dextran standard curve.

Pore Size Analysis via cryo-SEM: 51, 230, and 410 kDa HA-SH gels were prepared as described above and directly used for cryo-SEM analysis. Samples were fixed in a sandwich of 3 mm aluminum plates in a 2 mm notch and slushed nitrogen at −210 °C was used for rapid freezing. An EM VCT100 cryo-shuttle (Leica Microsystems) at −140 °C was used for all following transfer steps. One aluminum plate was knocked off to generate a freshly fractured hydrogel surface and samples were freeze edged in an ACE400 sputter coater machine (Leica Microsystems) under high vacuum ($<1 \times 10^3$ mbar) for 15 min at −85 °C. Afterward, samples were sputtered with 2.5 nm platinum before placing them into the SEM chamber (Crossbeam 340, Zeiss). Imaging was performed at −140 °C at an acceleration voltage of 8 kV.

Cell Viability Analysis: 3D constructs with encapsulated MSCs were washed with PBS before adding the live/dead staining solution (4×10^{-6} M ethidium homodimer III (EthD-III) and 2×10^{-6} M calcein acetoxymethylester (calcein-AM) in PBS; PromoKine, Heidelberg, Germany). After incubation for 45 min at rt in the dark, constructs were washed again with PBS and images were taken at a fluorescence microscope (Olympus BX51/DP71, Olympus, Hamburg, Germany). For quantification, three constructs per condition were imaged and living and dead cells were counted manually on at least 12 images per condition with the cell counter plugin of the NIH ImageJ Fiji software (version 1.52a).

Histological and Immunohistochemical Analysis: Histology and immunohistochemistry of MSC-laden 3D constructs were performed as previously described.[15] In brief, for all histological methods, sections with 8 μm thickness were mounted on SuperFrost plus glass slides (R. Langenbrick, Emmendingen, Germany). Collagen was stained with picrosirius red (0.1% direct red 80 in a saturated solution of picric acid), cells were counterstained with Weigert's hematoxylin. For staining of GAG, 0.1% safranin O was used, and cells were counterstained with 0.02% fast green. For immunohistochemistry the following primary antibodies were used: anti-aggrecan 969D4D11 (1:200; Thermo Scientific, Waltham, MA); anti-collagen type I ab34710 (1:200; Abcam, Cambridge, UK); anti-collagen type II clone II-4C11 (1:1000; Abnova, Taipei, Taiwan); and as a secondary antibody: goat-anti-mouse Alexa488 111-545-003 (1:400; Jackson ImmunoResearch, Cambridge, UK); all diluted in 1% BSA/PBS. Sections were mounted with DAPI mounting medium and analyzed with a fluorescence microscope. For quantification of the stained gel areas, cross sections from all areas of the construct were used. The values represent the average staining area of ten randomly taken images of each condition. All microscopic images were transformed to binary images and analyzed with the particle analysis function of the NIH ImageJ Fiji software (version 1.52p) using a 10% threshold of the maximal white value.[38]

Biochemical Analysis: MSC-laden 3D printed constructs, harvested on day 1 or 21, were homogenized for 5 min at 25 Hz before digesting the suspension with 3 U mL^{-1} papain for 20 h at 60 °C. Quantification of DNA,[39] GAG,[40] and collagen content[41,42] was performed after established protocols, with slight alterations as previously described.[15] Additionally, for quantification of total GAG and collagen production, culture supernatants of three replicates per condition were harvested every 2 d during culture and analyzed with the same protocols.

RNA Isolation and Gene Expression Analysis: RNA was isolated from 3D constructs with encapsulated MSCs on day 1, 7, and 21 using TRIzol reagent (Life Technologies, Carlsbad, CA) according to the manufacturer's instructions. Yield and purity of resulting RNA samples were assessed with a NanoDrop (Thermo Scientific, Waltham, MA) and cDNA was transcribed with the High-Capacity cDNA Reverse Transcription Kit (Applied Biosystems, Foster City, CA). For qRT-PCR, a CFX96 Real-Time System (Bio-Rad, Hercules, CA) and MESA GREEN qPCR Mastermix Plus for SYBR Assay (Eurogentec, Liège, Belgium) was used. Sequences of self-designed primer pairs for SOX9, ACAN, COL1A1, COL2A1, and GAPDH expression analysis are listed in Table S3 (Supporting Information). Relative expression was calculated using the $2^{-\Delta\Delta CT}$ method[43] and all samples were normalized to the housekeeping gene GAPDH and to gene expression of MSC 2D samples on d0.

Mechanical Analysis: Constructs were prepared in a defined cylindrical geometry (diameter: 5 mm, volume: 40 μL) and six constructs per condition were analyzed at day 1 and 21 of chondrogenic differentiation with a dynamical mechanical testing machine (ElectroForce 5500 test instrument, Bose, Eden Prairie, MN) with a load cell of 250 g. Compression of the constructs was performed with a constant crosshead displacement rate of 0.001 mm s^{-1} to a final depth of 0.5 mm and the Young's modulus was determined as the slope of the true stress–strain curve in the linear elastic range.

Statistical Analysis: Data are represented as mean ± standard deviation of at least three replicates, and statistical analysis was performed with GraphPad Prism 5 software. One-way ANOVA with a Bonferroni post hoc test was performed when comparing multiple groups at one time point. For comparing multiple groups at different time points, two-way ANOVA with Bonferroni post hoc test was used. Significant differences were marked as follows: $*p < 0.05$), $**p < 0.01$, and $***p < 0.001$.

Supporting Information

Supporting Information is available from the Wiley Online Library or from the author.

Acknowledgements

J.H. and L.F. contributed equally to this work. This work was funded by the Deutsche Forschungsgemeinschaft (DFG, German Research Foundation) [Project No. 326998133 – TRR 225 (subprojects A02, A06, B02, and C02)]. This work was further supported by the DFG within the "State Major Instrumentation Programme," providing funding for the SEM Crossbeam 340 (Zeiss) (Funding No. INST 105022/58-1 FUGG). The authors thank the Orthopedic Centre for Musculoskeletal Research, University of Würzburg, for providing bone samples; Jan Weichhold, Chair for Functional Materials in Medicine and Dentistry and Bavarian Polymer Institute, University of Würzburg, for designing the extrudability test setup; Malte Mildner, Institute of Organic Chemistry, University of Würzburg, for 400 MHz NMR measurements; and Jonas Hazur, Institute of Biomaterials, Friedrich-Alexander-University Erlangen-Nürnberg, for grid and filament fusion test G-codes.

Open Access funding enabled and organized by Projekt DEAL.

Conflict of Interest

The authors declare no conflict of interest.

Data Availability Statement

Research data are not shared.

Keywords

biofabrication, chondrogenic differentiation, dual-stage crosslinking, extracellular matrix, hyaluronic acid

Received: August 18, 2021
Revised: October 22, 2021
Published online: November 25, 2021

[1] J. Groll, T. Boland, T. Blunk, J. A. Burdick, D.-W. Cho, P. D. Dalton, B. Derby, G. Forgacs, Q. Li, V. A. Mironov, L. Moroni, M. Nakamura, W. Shu, S. Takeuchi, G. Vozzi, T. B. F. Woodfield, T. Xu, J. J. Yoo, J. Malda, *Biofabrication* **2016**, *8*, 013001.
[2] J. Groll, J. A. Burdick, D.-W. Cho, B. Derby, M. Gelinsky, S. C. Heilshorn, T. Jüngst, J. Malda, V. A. Mironov, K. Nakayama, A. Ovsianikov, W. Sun, S. Takeuchi, J. J. Yoo, T. B. F. Woodfield, *Biofabrication* **2018**, *11*, 013001.
[3] W. Sun, B. Starly, A. C. Daly, J. A. Burdick, J. Groll, G. Skeldon, W. Shu, Y. Sakai, M. Shinohara, M. Nishikawa, J. Jang, D.-W. Cho, M. Nie, S. Takeuchi, S. Ostrovidov, A. Khademhosseini, R. D. Kamm, V. Mironov, L. Moroni, I. T. Ozbolat, *Biofabrication* **2020**, *12*, 022002.
[4] R. Levato, T. Jungst, R. G. Scheuring, T. Blunk, J. Groll, J. Malda, *Adv. Mater.* **2020**, *32*, 1906423.
[5] B. S. Kim, S. Das, J. Jang, D.-W. Cho, *Chem. Rev.* **2020**, *120*, 10608.
[6] J. Malda, J. Visser, F. P. Melchels, T. Jüngst, W. E. Hennink, W. J. A. Dhert, J. Groll, D. W. Hutmacher, *Adv. Mater.* **2013**, *25*, 5011.
[7] D. Petta, U. D'amora, L. Ambrosio, D. W. Grijpma, D. Eglin, M. D'este, *Biofabrication* **2020**, *12*, 032001.
[8] V. H. M. Mouser, R. Levato, L. J. Bonassar, D. D. D'lima, D. A. Grande, T. J. Klein, D. B. F. Saris, M. Zenobi-Wong, D. Gawlitta, J. Malda, *Cartilage* **2017**, *8*, 327.
[9] J. A. Burdick, G. D. Prestwich, *Adv. Mater.* **2011**, *23*, H41.
[10] L. Bian, C. Hou, E. Tous, R. Rai, R. L. Mauck, J. A. Burdick, *Biomaterials* **2013**, *34*, 413.
[11] I. E. Erickson, A. H. Huang, S. Sengupta, S. Kestle, J. A. Burdick, R. L. Mauck, *Osteoarthritis Cartilage* **2009**, *17*, 1639.
[12] S. J. Bryant, K. S. Anseth, D. A. Lee, D. L. Bader, *J. Orthop. Res.* **2004**, *22*, 1143.
[13] B. M. Richardson, D. G. Wilcox, M. A. Randolph, K. S. Anseth, *Acta Biomater.* **2019**, *83*, 71.
[14] M. L. Vainieri, A. Lolli, N. Kops, D. D'atri, D. Eglin, A. Yayon, M. Alini, S. Grad, K. Sivasubramaniyan, G. J. V. M. Van Osch, *Acta Biomater.* **2020**, *101*, 293.
[15] J. Hauptstein, T. Böck, M. Bartolf-Kopp, L. Forster, P. Stahlhut, A. Nadernezhad, G. Blahetek, A. Zernecke-Madsen, R. Detsch, T. Jüngst, J. Groll, J. Teßmar, T. Blunk, *Adv. Healthcare Mater.* **2020**, *9*, 2000737.
[16] S. Stichler, T. Böck, N. Paxton, S. Bertlein, R. Levato, V. Schill, W. Smolan, J. Malda, J. Teßmar, T. Blunk, J. Groll, *Biofabrication* **2017**, *9*, 044108.
[17] C. Antich, J. de Vicente, G. Jiménez, C. Chocarro, E. Carrillo, E. Montañez, P. Gálvez-Martín, J. A. Marchal, *Acta Biomater.* **2020**, *106*, 114.
[18] E. Liao, M. Yaszemski, P. Krebsbach, S. Hollister, *Tissue Eng.* **2007**, *13*, 537.
[19] J. Lee, S.-H. Lee, B. S. Kim, Y.-S. Cho, Y. Park, *Tissue Eng. Regener. Med.* **2018**, *15*, 761.
[20] E. A. Kiyotake, A. W. Douglas, E. E. Thomas, S. L. Nimmo, M. S. Detamore, *Acta Biomater.* **2019**, *95*, 176.
[21] Q. Xu, S. A, P. Mcmichael, J. Creagh-Flynn, D. Zhou, Y. Gao, X. Li, X. Wang, W. Wang, *ACS Macro Lett.* **2018**, *7*, 509.
[22] M. Kesti, M. Müller, J. Becher, M. Schnabelrauch, M. D'este, D. Eglin, M. Zenobi-Wong, *Acta Biomater.* **2015**, *11*, 162.
[23] L. Ouyang, C. B. Highley, C. B. Rodell, W. Sun, J. A. Burdick, *ACS Biomater. Sci. Eng.* **2016**, *2*, 1743.
[24] D. Petta, A. R. Armiento, D. Grijpma, M. Alini, D. Eglin, M. D'este, *Biofabrication* **2018**, *10*, 044104.
[25] K. P. Vercruysse, D. M. Marecak, J. F. Marecek, G. D. Prestwich, *Bioconjugate Chem.* **1997**, *8*, 686.
[26] X. Z. Shu, Y. Liu, Y. Luo, M. C. Roberts, G. D. Prestwich, *Biomacromolecules* **2002**, *3*, 1304.
[27] J. W. Kuo, G. D. Prestwich, in *Comprehensive Biomaterials* (Ed: P. Ducheyne), Elsevier, Oxford **2011**, p. 239.
[28] G. M. Cruise, D. S. Scharp, J. A. Hubbell, *Biomaterials* **1998**, *19*, 1287.
[29] M. Iijima, D. Ulkoski, S. Sakuma, D. Matsukuma, N. Nishiyama, H. Otsuka, C. Scholz, *Polym. Int.* **2016**, *65*, 1132.
[30] B. L. Barthel, D. L. Rudnicki, T. P. Kirby, S. M. Colvin, D. J. Burkhart, T. H. Koch, *J. Med. Chem.* **2012**, *55*, 6595.
[31] L. Ambrosio, A. Borzacchiello, P. Netti, L. Nicolais, *J. Macromol. Sci., Part A* **1999**, *36*, 991.
[32] M. P. Lutolf, N. Tirelli, S. Cerritelli, L. Cavalli, J. A. Hubbell, *Bioconjugate Chem.* **2001**, *12*, 1051.
[33] P. Mesquida, D. Kohl, O. G. Andriotis, P. J. Thurner, M. Duer, S. Bansode, G. Schitter, *Sci. Rep.* **2018**, *8*, 10126.
[34] C. G. Pfeifer, A. Berner, M. Koch, W. Krutsch, R. Kujat, P. Angele, M. Nerlich, J. Zellner, *Materials* **2016**, *9*, 381.
[35] C. Chung, J. A. Burdick, *Tissue Eng., Part A* **2009**, *15*, 243.
[36] C. B. Knudson, W. Knudson, *Clin. Orthop. Relat. Res.* **2004**, *427*, S152.
[37] A. J. Engler, S. Sen, H. L. Sweeney, D. E. Discher, *Cell* **2006**, *126*, 677.
[38] E. C. Jensen, *Anat. Rec.* **2013**, *296*, 378.
[39] Y.-J. Kim, R. L. Y. Sah, J.-Y. H. Doong, A. J. Grodzinsky, *Anal. Biochem.* **1988**, *174*, 168.
[40] R. Farndale, D. Buttle, A. Barrett, *Biochim. Biophys. Acta* **1986**, *883*, 173.
[41] J. F. Woessner, *Arch. Biochem. Biophys.* **1961**, *93*, 440.
[42] A. P. Hollander, T. F. Heathfield, C. Webber, Y. Iwata, R. Bourne, C. Rorabeck, A. R. Poole, *J. Clin. Invest.* **1994**, *93*, 1722.
[43] K. J. Livak, T. D. Schmittgen, *Methods* **2001**, *25*, 402.